N91-15621

# A Phenomenological Approach to Multisource Data Integration: Analysing Infrared and Visible Data

N. Nandhakumar
Electrical Engineering Dept., Univ. of Virginia, Charlottesville, VA 22903

**Abstract**

A new method is described for combining multisensory data for remote sensing applications. The approach uses phenomenological models which allow the specification of discriminatory features that are based on intrinsic physical properties of imaged surfaces. Thermal and visual images of scenes are analyzed to estimate surface heat fluxes. Such analysis makes available a discriminatory feature that is closely related to the thermal capacitance of the imaged objects. This feature provides a method for labelling image regions based on physical properties of imaged objects. This approach is different from existing approaches which use the signal intensities in each channel (or an arbitrary linear or nonlinear combination of signal intensities) as features - which are then classified by a statistical or evidential approach.

## 1 Introduction

Multispectral/multisource data acquired via remote sensing have been shown to be useful for a variety of applications such as urban land-cover assessment, rain-rate classification, crop assessment, geophysical investigation, and surveillance and monitoring for national defence activities. Various techniques have been developed for combining the information in the different sensing modalities. These techniques typically use statistical or evidential rules to achieve the desired classification.

The usual statistical approach consists of first forming a feature vector wherein each element corresponds to the signal value (pixel gray level) from each sensor. This feature vector is then classified by a statistical decision rule. Other features such as the mean intensity level in a beighborhood, contrast, second and higher order moments, entropy measures, etc. have also been used as elements of the feature vector, e.g. [1]. In such approaches, interpretation of the imaged scene based on the fusion of information from the different sensors may be said to occur at the lower levels of analysis. In some techniques, linear and/or nonlinear combinations of signal values from different sensors form a feature, several of which are then fed to a classifier, e.g. [2]. In the latter case, interpretation may be said to occur at higher levels of analysis, after an earlier stage of information fusion which extracts discriminatory features. Other extensions to the standard statistical approach have been reported, e.g., a fuzzy relaxation labelling approach for image interpretation has been reported [3] wherein a Gaussian maximum likelihood classifier is used to provide initial probability estimates to the relaxation process.

Different optimal classification rules have been developed for interpreting multisource data for each of a variety of statistical models assumed for the data. The classifiers however do not address the problem of choosing *sufficiently* discriminatory features from the infinite number of available features. Such approaches therefore suffer from the disadvantage that the global optimality of the feature set is impossible to guarantee. Also, training of such classifiers is difficult since very large training data sets are warranted for achieving a reasonable error rate. It is also not clear what physical properties of the imaged objects are being utilized by the classifier during the discrimination process.

Evidential approaches have also been developed for combining information from multiple sensing

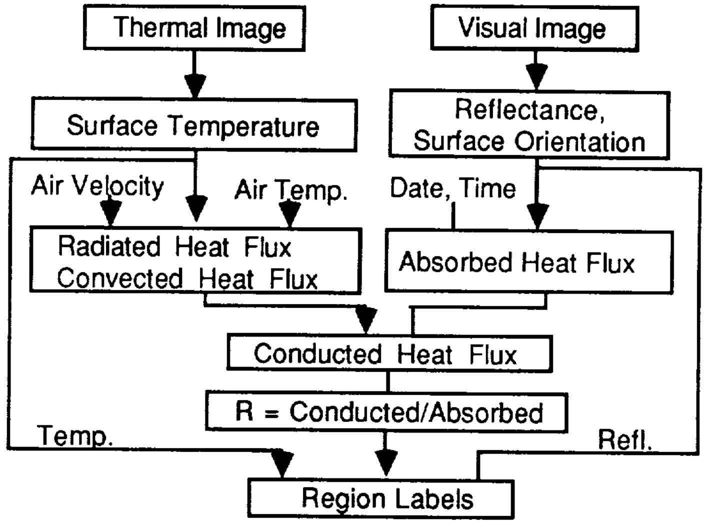


Figure 1. Combining thermal and visible data for surface heat flux estimation.

modalities, e.g. [4]- [6]. Such methods rely on a large set of heuristics rules which examine local contrast measures for each sensor and compare outputs from different sensors to provide varying degrees of support (certainty values) for a hypothesized class. A non-probabilistic framework is used for updating these uncertainties to reach a final classification. Interpretation in such systems is attempted at multiple levels of analysis. The rules, however, are based on manifestations of the differences in the intrinsic physical properties of objects rather than on direct measures of the physical properties themselves. Such approaches therefore do not fully exploit the synergy available in multisensor data fusion.

Due to these reasons, it is desirable to first combine information from the different sensors based on a physical model of the scene with the objective of evaluating intrinsic physical properties of the imaged objects. Such an analysis allows for specification of physically meaningful and discriminatory features which may then be used for scene interpretation by a probabilistic or evidential classifier at higher levels of analysis.

This paper discusses the development and use of phenomenological scene-sensor models for the fusion of information from infrared (IR) and visible data. A computational model is established in which principles of heat transfer are used along with computer vision techniques to derive a map of heat sinks and sources in the scene. The approach uses infrared imagery sensed in the $8\mu m$ – $12\mu m$ band, monochrome visual imagery, and knowledge of ambient conditions at the imaged surface to estimate surface heat fluxes in the scene. A feature which quantifies the surface's ability to sink/source heat radiation is derived and is shown to be useful in discriminating between different types of material classes such as vegetation and pavement.

It is assumed that the thermal image is segmented into closed regions by a suitable segmentation algorithm (e.g., [7]) and that the thermal and visual images are registered. The thermal image is processed to yield estimates of object surface temperature. This process requires the formulation of an appropriate model which relates scene radiosity to surface temperature, and received irradiation at the thermal camera to scene radiosity. Several object and scene parameters such as surface reflectivity, emissivity, reflected scene radiosity are incorporated in the model. The visual image, which is spatially registered with the thermal image, yields information regarding the relative surface orientation of the imaged object. The Lambertian reflectance model is used along with the shape-from-shading principle for this purpose. The above information along with information regarding ambient temperature, wind speed, and the date and time of image acquisition is used in a computational model that allows estimation of surface heat fluxes in the scene. The estimated surface heat fluxes are used to evaluate a feature that is closely related to the lumped thermal capacitance of the object. This feature is shown to be a meaningful and discriminatory feature for scene interpretation. A block diagram of the approach is shown in figure 1.

Multisensory images, and in particular - thermal and visual images, have been used in the past for evaluating a rough estimate of thermal inertia for various remote sensing applications [8] - [10]. The previously developed methods use very simple models of the scene and of the energy exchange phenomena ocurring at the imaged scene. In contrast to these past approaches, the technique developed in this paper is based on an explicit and more detailed physical model of the energy exchange in the scene and provides more meaningful and discriminatory features for classification.

The remainder of this paper is organized as follows. Section 2 describes an approach for extracting accurate surface temperature estimates from infrared imagery. Section 3 discusses the computation of relative surface orientation from visual imagery. Section 4 describes the estimation of surface heat fluxes at the imaged scene. Section 5 discusses two different ways of using the surface heat flux estimates for scene interpretation. Section 6 presents experimental results using real data, and section 7 contains a summary of the ideas presented in this paper.

## 2 Estimating Temperature from Thermal Images

A quantitative model has been derived for estimating the surface temperature of a viewed object using the thermal image. Details of the derivation may be found in reference [11]. The salient points of this model are presented below. The model is based on observations that are unique to the situation where outdoor scenes are illuminated by solar radiation. The derivation of the model rests on the following observations and results:

1. Most surfaces found in outdoor scenes may be considered to be diffuse emitters in the $8\mu m - 12\mu m$ band. Furthermore, they possess high emissivities in this band - in the range of 0.82 to 0.96. Hence, a constant value of 0.9 may be assumed for the IR emissivity of all imaged surfaces in outdoor scenes.

2. The radiosity of an object's suface in a natural scene comprises surface emission, reflected solar radiation, and reflection of radiation that emanates from other surfaces. These components contribute to the total irradiation at the IR detector. Only 0.1% of the total solar energy lies in the $8\mu m - 12\mu m$ band. Furthermore, the surface reflectivities to IR radiation are very low. On the other hand, a large percentage of emission from scene objects lies in the $8\mu m - 12\mu m$ band since their surface temperatures lie typically between 250K and 350K. Since IR emissivities are also high the scene irradiation at the IR detector is dominated by emission from the surface of the imaged object. The components due to reflected solar radiation and reflected emissions from other objects may be safely ignored.

3. The view factor $F_{oc}$ between the camera and imaged surface depends on the viewing geometry and typically involves the evaluation of complex integrals [12]. A reasonable approximation to

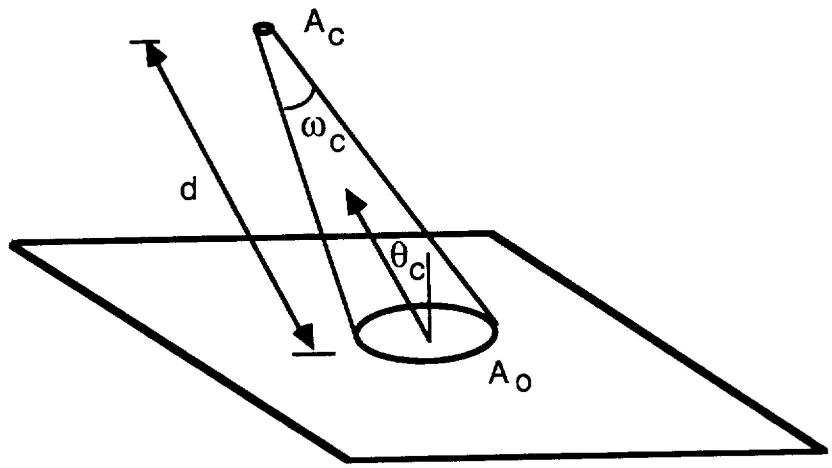


Figure 2. View factor between camera and imaged surface. $A_c$ is the circular viewing surface of the detector, $\omega_c$ is the solid angle subtended by the detector, $A_o$ is projection of $A_c$ onto the imaged surface, $d$ is the distance between the camera and the imaged surface, and $\theta_c$ is the angle between the surface normal and the viewing direction.

$F_{oc}$ is arrived at by making the following observations. Since the solid angle subtended by the detector $\omega_c$ is usually very small (on the order of 2 mrad) we can approximate the projection of the detector's viewing surface onto the imaged surface to be a planar circular patch, denoted by $A_o$ in figure 2.

The approximations indicated above allow for the derivation of a simple model that relates the surface temperature of the imaged object to the digitized value of the IR sensor's signal due to irradiation at the sensor [11]. The resulting model is expressed as:

$$0.9 \int_{\lambda_1}^{\lambda_2} \frac{C_1}{\lambda^5(exp(C_2/\lambda T) - 1)} d\lambda = K_a L_t + K_b \tag{1}$$

where, $C_1$ and $C_2$ are constants in Planck's equation and have values: $C_1 = 3.742 \times 10^8 \ W\mu m/m^2$ and $C_2 = 1.439 \times 10^4 \ \mu mK$. $T$ is the surface temperature of the imaged object, $\lambda$ is the wavelength of energy, $\lambda_1 = 8\mu m$ and $\lambda_2 = 12\mu m$. $L_t$ is the pixel gray level value of the digitized thermal image. $K_a$ and $K_b$ are constants for a particular imaging setup and are obtained by appropriate camera calibration as described below.

The model established above provides a simple algorithm for surface temperature estimation. At the outset a table of values of $F(T_i) = 0.9 \int_{\lambda_1}^{\lambda_2} \frac{C_1}{\lambda^5(exp(C_2/\lambda T_i)-1)} d\lambda$ is created for different values of $T_i$ via numerical integration of this expression. A scene containing two objects at two different known temperatures is imaged. The corresponding gray level values are used in equation (1) to solve for the constants $K_a$ and $K_b$. Thereafter, the temperature of other surfaces in other scenes can be determined by first evaluating the right-hand side of equation (1) using the corresponding gray level. Then the table of values of $F(T_i)$ created above is looked up for a matching value. The value of the associated index $T_i$ now provides the surface temperature estimate.

In general, an exact match will not be found and a linear interpolation is performed as follows to acquire a reasonably accurate estimate of the surface temperature. Consider a particular gray level value $L_t$ in the thermal image which corresponds to a surface temperature of $T_s$. Let the right-hand side of equation (1) evaluate to $G$, i.e., $G = K_a L_t + K_b$. On searching for a match in the table of values of $F(T_i)$ assume that $G$ is found to lie between adjacent entries $F(T_m)$ and $F(T_n)$ such that $F(T_m) < G < F(T_n)$. The desired value of surface temperature is then computed as:

$$T_s = T_m + \frac{T_n - T_m}{F(T_n) - F(T_m)}(G - F(T_m)) \tag{2}$$

In deriving the above approach for temperature estimation, the effect of atmospheric attenuation has been ignored. This is justifiable for the following imaging situations:

1. The surfaces whose temperatures are to be estimated appear in the same scene that was used for calibration.
2. The distance between the calibration surfaces and the thermal camera is the same as the distance between the surfaces whose temperatures are to be estimated and the camera.
3. The distance between imaged surfaces and the thermal camera is on the order of only a few hundred meters [13].

If neither of the above conditions apply, appropriate models need to be applied to account for atmospheric attenuation loss [13]- [15].

# 3 Inferring Surface Reflectivity and Relative Orientation

In order to estimate heat fluxes it is necessary to estimate not only surface temperature as described above but also surface reflectance to visible radiation and also surface orientation relative to the incident (solar) radiation. The visual image of the scene provides clues to both these quantities. In the following discussion it is assumed that the infrared and visual images of a scene are spatially registered, and that the images are segmented *a priori* into regions by a method such as that described in [7].

The use of shading information to recover the shape of an object has been addressed by several researchers, e.g. [16]-[20]. These techniques, however, can be applied only if certain conditions are satisfied. The bi-directional reflectance distribution function of the surface must be known *a priori.* Image resolution must be high enough to allow the rendition of several surface patches near the occluding boundary, or there need to exist background patches of known surface orientation surrounding the region of unknown surface orientation. These conditions are difficult to satisfy when imaging objects in a natural scene. We also note that while the aforesaid efforts attempt the problem of determining the $(x, y, z)$ direction cosines of the surface normals of the imaged surface, our problem is a much simpler one, i.e., to arrive at an accurate estimate of $cos\theta_i$, where $\theta_i$ is the angle between the surface normal and the direction of incident radiation. A simpler method may be used for this purpose as described below.

Real surfaces in outdoor scenes exhibit a combination of diffuse and specular reflectivities. The diffuse component has been found to dominate in commonly occurring surfaces [21]. Hence, it is reasonable to assume that the imaged surfaces are Lambertian reflectors. If $L_v$ represents the gray level of a pixel in the visual image, the relative surface orientation of the surface patch corresponding to that pixel is related to the brightness value by:

$$L_v = K_\rho \, cos\theta_i \; + \; C_v \tag{3}$$

where, $K_\rho = \rho \; K_v$, $\rho$ is the surface reflectance, $K_v$, $C_v$ are constants of the visual imaging system and are determined via calibration. The calibration process simply consists of imaging two different surfaces at known orientations to solar radiation and of known reflectivities, whence the constants $K_v$ and $C_v$ are easily computed.

It is possible to obtain via stereoscopic image analysis, laser radar imagery, or from registered digital terrain data, the orientation of one elemental surface patch in the entire surface that is represented by a given image region. This orientation is best acquired for the elemental area that provides a reliable estimate, e.g., one that lies within a large planar patch. The region reflectivity $\rho$ is then computed using equation (3). Knowing $\rho$, the value of $cos\theta_i$ is easily computed at each pixel in that region using equation (3). The surface is assumed to be opaque, hence, the absorptivity is computed as $\alpha_s = 1 - \rho$. The above procedure is applied to each region in the image to provide estimates of $\rho$ and $cos\theta_i$ at each pixel in the entire image.

The assumption that viewed surfaces are opaque and are Lambertian is sometimes violated by the presence of transparent objects (e.g. glass windows, lakes), or regions of specular reflection (e.g. a polished surface). It is assumed that such regions in the imagery are detected by means other than that presented in this paper.

## 4 Estimating Surface Heat Fluxes

In this section, the various heat fluxes at the surface of the object are identified and the relationship between them is specified. A method for estimating these heat fluxes is then presented. This method uses values of surface temperature deduced from the thermal image, and surface reflectivity and relative orientation deduced from the visual image. Section 5 describes methods for interpreting imaged scenes using these heat flux estimates.

Consider an elemental area on the surface of the imaged object. Assuming one-dimensional heat flow, the heat exchange at the surface of the object is represented by figure 3. $W_i$ is the incident solar radiation, $\theta_i$ is the angle between the direction of irradiation and the surface normal, the surface temperature is $T_s$, and $W_{abs}$ is that portion of the irradiation that is absorbed by the surface. $W_{cv}$ denotes the heat convected from the surface to the air which has temperature $T_{amb}$ and velocity $V$, $W_{rad}$ is the heat lost by the surface to the environment via radiation and $W_{cd}$ denotes the heat conducted from the surface into the interior of the object. Irradiation at the object surface also includes that emanating from other scene components. As discussed in section 2, the magnitude of this absorbed irradiation is small when compared to total solar irradiation absorbed in visible and IR bands. The contribution of the former may therefore be ignored.

At any given instant, applying the law of conservation of energy to the heat fluxes flowing into the surface of the object and those flowing out from the surface. we have,

$$W_{abs} \;=\; W_{cd} \;+\; W_{cv} \;+\; W_{rad} \tag{4}$$

where, $W_{rad} \;=\; 0.9 \, \sigma \, (T_s^4 - T_{amb}^4)$,

$$W_{abs} \;=\; W_i \; cos\theta_i \; \alpha_s \; , \tag{5}$$

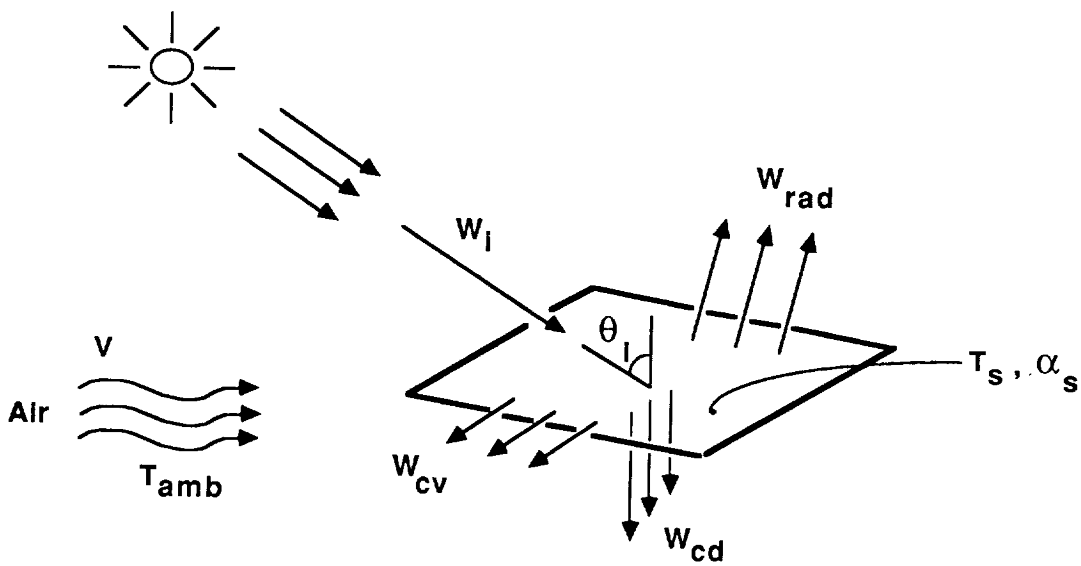


Figure 3. Exchange of heat fluxes at the surface of the imaged object.

$\sigma$ denotes the Stefan-Boltzman constant, and $\alpha_s$ denotes the solar absorptivity of the surface. The convected heat transfer is given by

$$W_{cv} = h(T_s - T_{amb}) \tag{6}$$

where, $h$ is the average convected heat transfer coefficient, and depends on the properties of the surrounding air (e.g. velocity, viscosity, temperature, etc.), and on the geometry and the nature of the object's surface. We note that $W_{rad}$ is immediately available when $T_{amb}$ is known since $T_s$ is deduced from the thermal image as discussed in section 2.

In order to estimate the heat flux absorbed by the surface, it is first neccesary to determine the magnitude of the incident radiation on a horizontal surface and then compensate for the orientation and the reflectivity of the imaged surface. One approach is to directly measure the incident solar radiation using a pyrheliometer. Alternately, as was done in the experiments described later, an appropriate analytical model may be used to estimate this quantity. The variation (with day of the year and time of day) of the intensity of solar radiation incident on a horizontal surface on the ground has been modelled by Thepchatri, *et al.* [22] based on the data presented by Strock and Koral [23]. The empirical model accounts for diurnal and seasonal variations. This model is used for specifying $W_i$. Thus, knowing $cos\theta_i$ and $\alpha_s$ as described in section 3, $W_{abs}$ may be computed using from equation (5).

The convective heat flux is obtained by using equation (6). The temperature for the object's surface is obtained from the thermal image as described in the previous section. The ambient temperature $T_{amb}$ is known. The problem therefore lies in estimating the average convected heat transfer coefficient $h$. A plethora of empirical correlations have been established for computing $h$ for various thermal and hydrodynamic conditions [24]. The simplifying assumption that the portion of the surface being viewed is flat allows the use of convecion correlations developed for external flow over flat plates [24]. The procedure for estimating the convected heat flux is as follows: knowing the wind velocity and the air temperature, the Reynolds number is computed, where the characteristic length of the object is

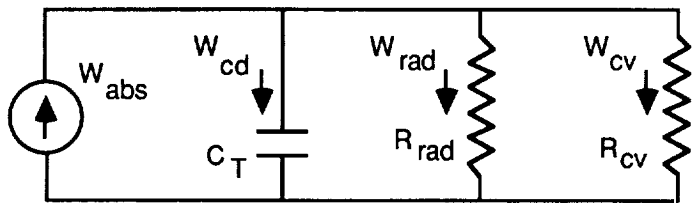


Figure 4. Equivalent thermal circuit of imaged surface.

assumed to be 1 meter. The value of the Reynolds number determines whether laminar or mixed flow conditions exist. Accordingly, the appropriate correlation is used. The Nusselt number is thus obtained and thence the convected heat transfer coefficient $h$. Equation (6) is now used to provide the estimate of convected heat flux.

Having estimated the convected heat flux, the radiated heat flux, and the absorbed irradiation as described above, the conduction heat flux is then deduced using equation (4).

# 5 Scene Interpretation

The estimated surface heat fluxes may be used to derive physically meaningful interpretations of the scene. Two different methods are discussed. The first approach assumes that only a single data set of the scene is available, and it consists of the thermal image, the visual image, and values of scene parameters obtained at a particular instant of time. The second method assumes that a sequence of data sets obtained at different time instants is available. The first approach is more suitable for scenes, the contents of which change frequently, e.g., one that contains automobiles. The second approach is suitable for scenes containing objects that are stationary over the sequence of data sets, e.g., scenes containing only vegetation, buildings and pavements.

## 5.1 Analysis of a Single Multisensory Data Set

The estimated surface heat fluxes may be used to evaluate how well an object can act as a heat source/sink. Thus a highly discriminatory feature may be extracted which is closely related to an intrinsic physical property of the imaged object. Considering a unit area on the surface of the imaged object, the equivalent thermal circuit for the surface is shown in figure 4. $C_T$ is the lumped thermal

| *Object* | *Thermal Capacitance* ($\times 10^{-6}$ Joules/Kelvin) |
|---|---|
| Asphalt Pavement | 1.95 |
| Concrete Wall | 2.03 |
| Brick Wall | 1.51 |
| Wood(Oak) Wall | 1.91 |
| Granite | 2.25 |
| Automobile | 0.18 |

Table 1: Normalized values of lumped thermal capacitance.

capacitance of the object and is given by

$$C_T = DVc$$

where, $D$ is the density of the object, $V$ is the volume, and $c$ is the specific heat. The resistances are given by:

$$R_{cv} = \frac{1}{h} \quad \text{and} \quad R_{rad} = \frac{1}{0.9\sigma(T_s^2 + T_{amb}^2)(T_s + T_{amb})}$$

From figure 4 it is clear that the conduction heat flux $W_{cd}$ estimated in the previous section depends on the lumped thermal capacitance $C_T$ of the object. A relatively high value for $C_T$ implies that the object is able to sink or source relatively large amounts of heat. An estimate of $W_{cd}$, therefore, provides us with a relative estimate of the thermal capacitance of the object, albeit a very approximate one. Table 1 lists values of $C_T$ of typical objects imaged in outdoor scenes. The values have been normalized for unit volume of the object.

Note that the thermal capacitance for walls and pavements is significantly greater than that for automobiles and hence $W_{cd}$ may be expected to be higher for the former regions. Plants absorb a significant percentage of the incident solar radiation. The energy absorbed is used for photosynthesis and also for transpiration. Only a small amount of the absorbed radiation is convected into the air. Therefore, the estimate of the $W_{cd}$ will be almost as large (typically 95%) as that of the absorbed heat flux. Thus, $W_{cd}$ is useful in estimating the object's ability to sink/source heat radiation, a feature shown to be useful in discriminating between different classes of objects. However, in order to minimize the feature's dependence on differences in absorbed heat flux, a normalized feature was defined to be the ratio

$$R = W_{cd}/W_{abs}$$

Although the heat flux ratio, $R = W_{cd}/W_{abs}$, does capture a great deal of information about the imaged object, it is not discriminatory enough to unambiguously delineate the identity of the imaged object. Other sources of information are therefore warranted. Hence, information such as the surface reflectivity, $\rho$, of the region which is derived from the visual image, and average region temperature which is derived from the thermal image are also used to facilitate region labeling. Section 6 presents experimental results of using this approach on real multisensory data.

## 5.2 Analysing Temporal Sequence of Multisensor Data

If a temporal sequence of multisensor data consisting of thermal imagery, visual imagery and scene conditions is available, then it is possible to extract a more reliable estimate of the imaged object's relative ability to sink/source heat radiation. Observe that the relationship between the conducted heat flux $W_{cd}$ and the thermal capacitance $C_T$ of the object is given by:

$$W_{cd} = C_T \frac{dT_s}{dt}$$

A finite (backward) difference approximation to this equation may be used for estimating $C_T$ as

$$C_T = W_{cd} \frac{(t_2 - t_1)}{(T_s(t_2) - T_s(t_1))} \tag{7}$$

where, $t_1$ and $t_2$ are the time instants at which the data were acquired, $T_s(t_1)$ and $T_s(t_2)$ are the corresponding surface temperatures, and $W_{cd}$ is the conducted heat flux which is assumed to be constant during the time interval. However, $W_{cd}$ does vary and an average value of $(W_{cd}(t_1) + W_{cd}(t_2))/2$ is used in equation (7).

Section 6 presents experimental results obtained by applying the above temporal analysis method to multisensory data.

## 6 Experimental Results

The methods described in the previous sections were applied to real multisensory data acquired from outdoor scenes. Calibrated remote sensing data were not available along with values of ambient scene parameters such as wind speed and temperature. Hence, thermal and visual imagery were acquired from a ground based imaging setup consisting of an Inframetrics infrared imaging system and a video imaging system. An anemometer was used to measure wind speed and a digital thermometer was used to calibrate the thermal imaging system so as to allow absolute temperature estimates as discussed in section 2. The two methods discussed in the previous section were applied to several sets of data which were acquired at different times of the day and during different seasons of the year.

The results obtained using one data set are presented in figures 5 through 8. Figure 5 shows the visual image of a scene containing an automobile, buildings, asphalt pavement and vegetation. Figure 6 shows the thermal image of the same scene. The techniques described in the preceeding sections of this paper were used to estimate the surface heat fluxes, whence the ratio $R = W_{cd}/W_{abs}$ was computed at each pixel. A histogram of these values was computed for each region and the mode of the histogram was found. This value was chosen as the representative value of $R$ for the region. Figure 7 shows the values obtained for each region. As predicted by the discussion in section 5, automobiles produce the lowest value of this feature, pavements and buildings produce intermediate values and vegetation produces the highest values.

In addition to the feature $R$, the average region temperature, and the surface reflectivity were also used in a decision tree classifier to label regions as building, pavement, vegetation or automobile. The classifier used heuristic rules of the form:
IF { $R \in [0.2, 0.9]$ AND $\rho \in [0.35, 1.0]$ } OR { $R \in [-.8, -.3]$ } THEN label = bldng
The resultant classification is shown in figure 8.

The method of temporal analysis of the scenes was tested on data acquired at intervals of three hours. Table 2 presents the mean and standard deviation of the value of $C_T$ estimated for different classes of scene objects. The estimated values compare very favorably with those listed in table 1. Except for the concrete and brick walls, the estimated values for each class are of the same order of

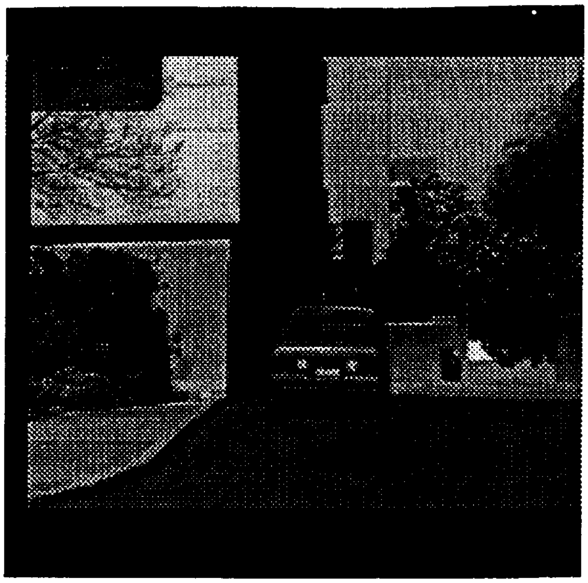

Figure 5. Visual image.

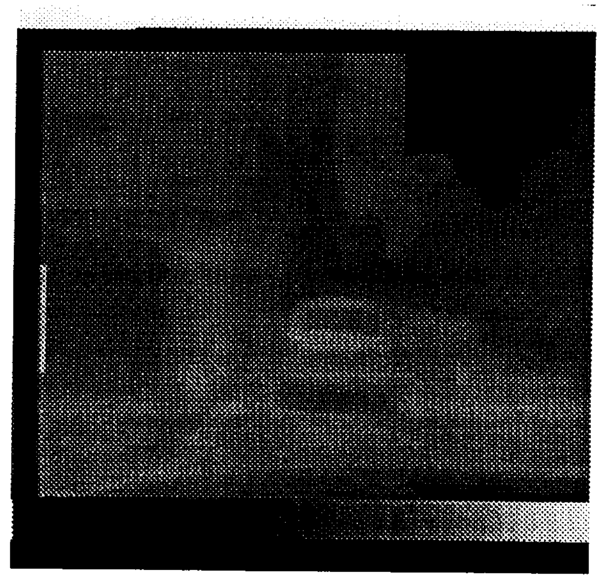

Figure 6. Thermal image.

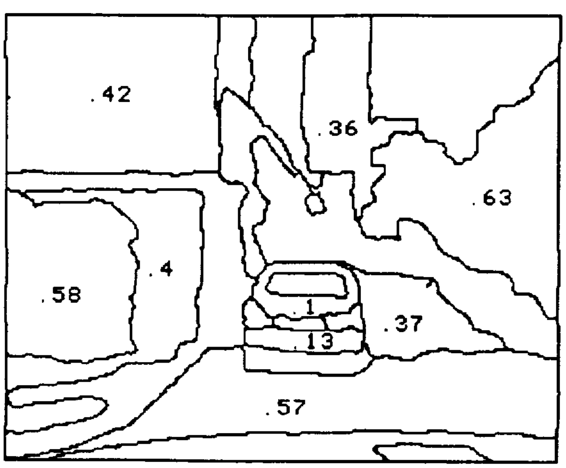


Figure 7. Mode of feature $R$.

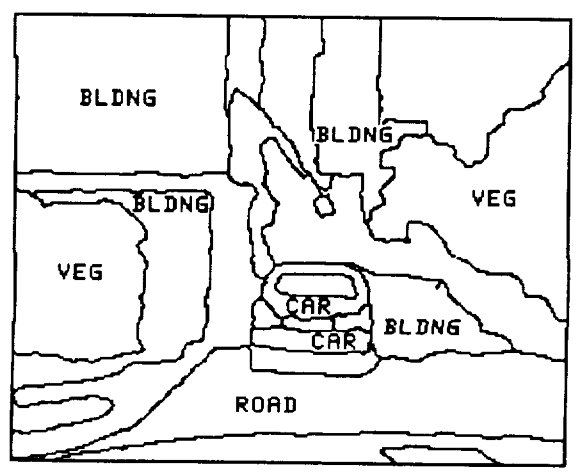


Figure 8. Region classification.

| *Object* | *Average $C_T$* ($\times 10^{-6}$ J/K) | Std. Devn. ($\times 10^{-6}$ J/K) |
|---|---|---|
| Automobile | 0.08 | 0.08 |
| Concrete Wall | 0.22 | 0.37 |
| Brick Wall | 0.37 | 0.38 |
| Asphalt Pavement | 1.05 | 0.46 |
| Vegetation | 1.5 | 2.7 |

Table 2: Values of lumped thermal capacitance estimated using the method described in section 5.2.

magnitude as listed in table 1, and are ordered in a similar manner. The walls do not compare favorably possibly due to the wide variation in wall thickness that is difficult to account for and also due to the unknown thermal conditions on the interior surface of the walls. In general, a significant offset may be expected in the estimated values due to the many approximations used in the computation of the heat flux estimates. Inspite of this limitation, it is obvious that the approach described above makes available a very useful and meaningful method for the interpretation of multisensory data. Note also that the value of $C_T$ is a deterministic value which is completely defined by a physical definition for a particular class of objects. Hence, a deterministic measure of the technique's performance is available by comparing the estimated and true values of $C_T$. Such a measure is not available in purely statistical interpretation techniques. This is one of the major advantages of a phenomenological approach to scene interpretation when compared to the purely statistical approach.

# 7 Conclusions

A new method has been described for interpreting scenes using multisensory data. The phenomenological approach combines information from the different imaging modalities to derive meaningful features. The approach is based on physical models of the energy exchange between the imaged surface and the environment. The thermal and visual images yield estimates of surface heat fluxes which in turn provide a measure of the relative ability of the imaged surface to source/sink heat energy. The interpretation thus relies on a rough estimate of the lumped thermal capacitance of the object which has been shown to vary widely for different classes of objects in outdoor scenes. The developed approach was tested on real multisensory data. Due to the unavailability of a calibrated remote sensing data and accompanying values of ambient scene conditions, the testing was performed using terrain based imaging equipment. The approach described above may be easily applied to multisensory imagery acquired by airborne or satellite-based sensors.

# References

[1] B.G. Lee, R.T. Chin and D.W. Martin, "Automated Rain-Rate Classification of Satellite Images Using Statistical Pattern Recognition", *IEEE Trans. Geoscience and Remote Sensing*, Vol. GE-23, No. 3, May 1985, pp. 315-324.

[2] W.D. Rosenthal, B.J. Blanchard and A.J. Blanchard, "Visible/Infrared/Microwave Agriculture Classification, Biomass and Plant Height Algorithms", *IEEE Trans. Geoscience and Remote Sensing*, Vol. GE-23, No. 2, March 1985, pp. 84-90

[3] S. Di Zenzo, R. Bernstein, S.D. Degloria and H.G. Kolsky, "Gaussian Maximum Likelihood and Contextual Classification for Multicrop Classification", *IEEE Trans. Geoscience and Remote Sensing*, Vol. GE-25, No.

6, Nov. 1987, pp. 805-814

[4] S.W. Wharton, "A Spectral Knowledge-Based Approach for Urban Land-Cover Discrimination", *IEEE Trans. Geoscience and Remote Sensing*, Vol. GE-25, No. 3, May 1987, pp. 272-282

[5] T. Lee, J.A. Richards, and P.H. Swain, "Probabilistic and Evidential Approaches for Multisource Data Analysis", *IEEE Trans. Geoscience and Remote Sensing*, Vol. GE-25, No. 3, May 1987, pp. 283-293

[6] D.G. Goodenough, M. Goldberg, G. Plunkett and J. Zelek, "An Expert System for Remote Sensing", *IEEE Trans. Geoscience and Remote Sensing*, Vol. GE-25, No. 3, May 1987, pp. 349-359

[7] H. Asar, N. Nandhakumar and J.K. Aggarwal, "Pyramid-Based Image Segmentation Using Multisensory Data", to appear in *Pattern Recognition.*

[8] V.S. Whitehead, W.R. Johnson and J.A. Boatright, "Vegetation Assessment Using a Combination of Visible, Near-IR and Thermal-IR AVHRR Data", *IEEE Trans. Geoscience and Remote Sensing*, Vol. GE-24, No. 1, Jan. 1986, pp. 107-112.

[9] P.R. Christensen, "Martian Dust Mantling and Surface Compositions: Interpretations of Thermophysical Properties", *Journal of Geophysical Research*, Vol. 87, No. B12, 1982, pp. 9985-9998.

[10] B.M Jakosky and P.R. Christensen, "Global Duricrust on Mars: Analysis of Remote Sensing Data", *Journal of Geophysical Research*, Vol. 91, No. B3, 1986, pp. 3547-3559.

[11] N. Nandhakumar and J.K. Aggarwal, "Integrated Analysis of Thermal and Visual Images for Scene Interpretation", *IEEE Trans. on Pattern Analysis and Machine Intelligence*, Vol. 10, No. 4, July 1988, pp. 469-481.

[12] R. Siegel and J.R. Howell, *Thermal Radiation Heat Transfer*, 2nd Ed., Mc-Graw Hill Book Co., New York, 1981.

[13] C. Ohman, "Practical Methods for Improving Thermal Measurements", *Proc. of SPIE*, Vol. 313, 1981, pp 204 - 212.

[14] J.R. Schott and J.D. Biegel, "Comparison of Modelled and Empirical Atmospheric Propagation Data", *Proc. of SPIE*, Vol. 430, 1983, pp 45 - 52.

[15] J.M. Jarem, J.H. Pierluissi and W.W. Ng, "A Transmittance Model for Atmospheric Methane", *Proc. of SPIE*, Vol. 510, 1984, pp 94 - 99.

[16] Horn B.K.P., and Sjoberg R.W., "Calculating the Reflectance Map", *Applied Optics*, Vol. 18, No. 1, 1979, pp 1770 - 1779.

[17] Horn B.K.P., "Hill Shading and the Reflectance Map", *Proc. of the IEEE*, Vol. 19, No. 1, pp 14 - 47.

[18] Woodham R.J., "Analysing Images of Curved Surfaces", *Artificial Intelligence*, Vol. 17, 1981, pp 117 - 140.

[19] Ikeuchi K., and Horn B.K.P., "Numerical Shape from Shading and Occluding Boundaries", *Artificial Intelligence*, Vol. 17, 1981, pp 141 - 184.

[20] R.T. Frankot and R. Chellappa, "A Method for Enforcing Integrability in Shape from Shading Algorithms", *IEEE Trans. on Pattern Analysis and Machine Intelligence*, Vol. 10, No. 4, July 1988, pp. 439-451.

[21] J.M. Norman, J.M. Welles and E.A. Walter, "Contrasts Among Bidirectional Reflectance of Leaves, Canopies and Soils", *IEEE Trans. Geoscience and Remote Sensing*, Vol. GE-23, No. 5, September 1985, pp. 659-667.

[22] Thepchatri T., Johnson C.P., and Matlock H., "Prediction of Temperature and Stresses in Highway Bridges by A Numerical Procedure Using Daily Weather Reports", Tech. Report 23-1, 1977, Center for Highway Research, University of Texas at Austin.

[23] Strock C., and Koral R. L., *Handbook of Air Conditioning, Heating and Ventilating*, Industrial Press, Inc., 2nd Ed., 1965.

[24] Incropera F.P., and De Witt D.P., *Fundamentals of Heat Transfer*, John Wiley & Sons, Inc., New York, 1981.